ACS OMEGA

Open Access

http://pubs.acs.org/journal/acsodf

Article

Hydrogen Bond and Dipole−Dipole Interaction Enabling Ultrastable, Quick Responding, and Self-Healing Proton Exchange Membranes for Fuel Cells

Shanyun Mo, Zihui Li, Junda Chen, Yue Chen, Ning Wang, Chunmei Tang, Ling Meng, Lei Du, Lixin Xing,* and Siyu Ye*

Cite This: *ACS Omega* 2024, 9, 26316−26324

Read Online

ACCESS | Metrics & More | Article Recommendations | Supporting Information

ABSTRACT: Proton exchange membranes (PEMs) are subject to mechanical degradation, such as microcracks and pinhole formation, under real-world fuel cell operating conditions, which leads to great issues in terms of device death and safety concerns. Therefore, PEMs with self-healing features are imperative but have rarely been used for proton exchange membrane fuel cells (PEMFCs). Here, a dimensionally stable and self-healing PEM is developed by tuning the hydrogen bond and dipole−dipole interactions between the mature perfluorinated sulfonic acid (PFSA) and a self-healing copolymer, which is specifically synthesized with hexafluorobutyl acrylate (HFBA) and acrylic acid (AA). This hexafluorobutyl acrylate-acrylic acid copolymer (HFBA-*co*-AA) is suggested as the key to improving the self-healing efficiency of the blended PFSA/HFBA-*co*-AA membrane. This PFSA/HFBA-*co*-AA membrane can recover 43.6% of the original tensile strength within only 20 min at 80 °C. This study may pave an avenue toward the development of reliable and durable PEM for fuel cells.

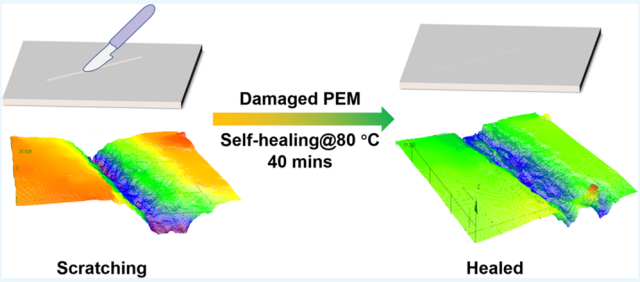

1. INTRODUCTION

Nowadays, hydrogen, as a clean energy resource, has regained great attention from industry, academia, and governments. Reasonably, hydrogen proton exchange membrane fuel cells (PEMFCs), which can directly convert chemical energy into electricity with high efficiency, high energy density, and zero carbon emission, have been pursued worldwide.[1−4]

As one of the most important components, proton exchange membrane (PEM) has presented a great influence on fuel cell performance and lifetime.[5] Many efforts have thus been devoted to developing advanced PEMs with superior proton conductivity, low gas permeability, and excellent durability.[6] Perfluorinated sulfonic acid (PFSA), including hydrophobic tetrafluoroethylene backbones with hydrophilic sulfonic acid groups (−SO_3H), has been widely used for PEMs.[7−10] To obtain superior PEMs, significant research efforts have been made. For example, the PEMs consisting of a polymeric phase hosting functional nanofillers are promising—the unique phase-separated architectures at polymer−nanofiller interfaces could promote proton transportation.[11] The nanofillers could be nanofibers,[12] the hygroscopic inorganic materials including ZrO_2, TiO_2, $TiSiO_4$, and silica,[13,14] the radical scavengers including CeO_x[15] structure enforced polytetrafluoroethylene,[16] metal−organic frameworks,[17] and even graphene oxide,[18] etc.

However, under the real-world operating conditions of PEMFC, for example, vehicle operating conditions, the local temperature and humidity usually fluctuate, leading to cyclical hydration and dehydration of PEMs.[19,20] As a result, the PEMs undergo repeated swelling and deswelling, easily generating microcracks and pinholes; particularly, these PEM defects are easily observed at the stress concentration area between frames and gas diffusion layers.[21,22] Such PEM degradation can not only lower performance but also increase the safety risk of massive gas permeation.[23−25] In this regard, it is highly desirable to develop PEMs with self-healing features to address mechanical damage problems.

To design a self-healing membrane, microcapsules containing healing agents can be used. Note that the employment of microcapsules may lead to open channels for gas to pass in the membranes; meanwhile, applying the microcapsule is a one-in-a-lifetime method—once the damage is healed, the microcapsule is out of work.[26] Thus, we prefer to design the membranes with intrinsic self-healing ability through reversible covalent bonds and noncovalent interactions.[27−29] Reasonably,

Received: March 7, 2024
Revised: May 21, 2024
Accepted: May 29, 2024
Published: June 7, 2024

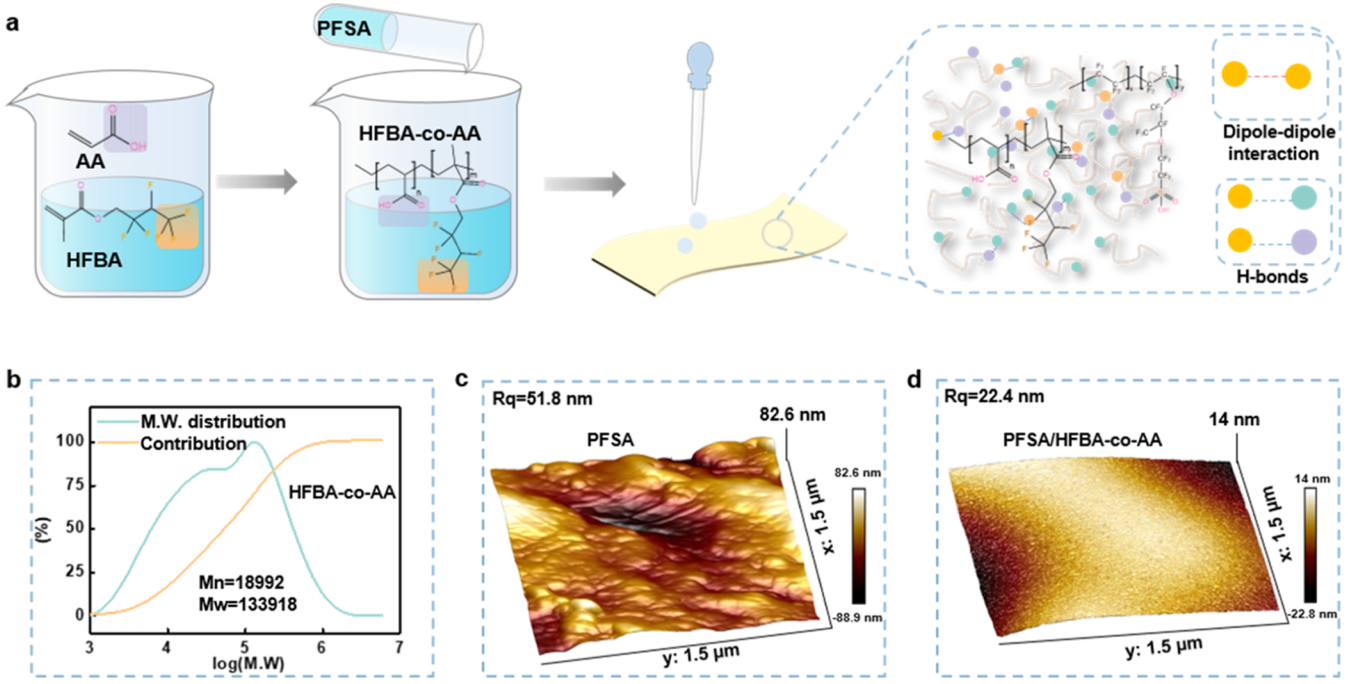

Figure 1. (a) The preparation process of the HFBA-*co*-AA and PFSA/HFBA-*co*-AA membrane. (b) GPC graph of HFBA-*co*-AA molecular weight and the distribution of molecular weight. AFM images of the (c) PFSA membrane and (d) PFSA/HFBA-*co*-AA membrane.

a desired self-healing polymer that can be blended with mature PFSA is required to realize the self-healing ability.

We summarized the details of representative works regarding self-healing membranes in Table S1. The majority of reported self-healing membranes are focused on direct methanol fuel cells or nonenergy areas.[27,30−33] These works are an excellent guide for our work, although the working conditions of these works are different from PEMFCs. On the other hand, the healing efficiency of the reported membranes is not high, for example, several hours are required to heal the damages.[29] Therefore, we herein target developing self-healing PEMs with a better self-healing efficiency.

Most reported self-healing ability of membranes originates from hydrogen bonds.[27,29,30,32,33] To enhance the self-healing efficiency, the strong dipole−dipole interaction of $-CF_3$ groups is particularly introduced by using the hexafluorobutyl acrylate (HFBA), a kind of all-dipole fluorine elastomer, as a self-healing polymer.[34−36] One of the benefits of employing HFBA is that both HFBA and PFSA have $-CF_3$ groups, likely promoting a self-healing performance once they are blended. However, the blended HFBA/PFSA membrane is soft and pretty weak in mechanical strength, probably because the HFBA chain is soft.[36] To precisely tune the mechanical feature, another monomer, acrylic acid (AA), is additionally used because the random copolymer usually has better mechanical strength.[37]

Accordingly, we design and synthesize a composite fluorine elastomer, i.e., the copolymer of hexafluorobutyl acrylate (HFBA) and acrylic acid (AA), namely, HFBA-*co*-AA. Specifically, 40 mmol of HFBA, 10 mmol of AA, and 0.25 mmol of azodiisobutyronitrile (AIBN) were mixed in a glass bottle and stirred for 30 min, followed by heating at 70 °C for 30 min. Next, 10.72 g of *N*,*N*-dimethylformamide (DMF) was added to HFBA-*co*-AA for 24 h to prepare the HFBA-*co*-AA solution. Whereafter, the PFSA/HFBA-*co*-AA composite membrane was prepared by directly mixing PFSA and HFBA-*co*-AA solution with a specific mass ratio under continuous string at room temperature. The mixture was then directly poured into a PTFE mold and dried in the oven at 150 °C for 60 min, forming a PFSA/HFBA-*co*-AA membrane. This membrane presents good self-healing properties; for example, 43.6% of the original tensile strength can be recovered within only 20 min at 80 °C, a mimic fuel cell working condition. This work suggests a potential membrane material for PEMFC applications.

2. RESULTS AND DISCUSSION

As discussed above, HFBA is employed as a self-healing polymer in this work, whose self-healing ability comes from the strong dipole−dipole interaction of the $-CF_3$ groups. However, the blended HFBA/PFSA membrane is found to be weak in mechanical strength (as shown in Figure S1, Supporting Information). To address this problem, another monomer, acrylic acid (AA), is selected to precisely tune the blended membrane. AA is chosen because the random copolymer usually has better mechanical strength. Meanwhile, the carboxyl groups of AA can act as auxiliary transport sites to jointly participate in the establishment of hydrophilic nanochannels,[38] which greatly contribute to proton conduction. Accordingly, we design and synthesize a composite fluorine elastomer, i.e., the copolymer of hexafluorobutyl acrylate (HFBA) and acrylic acid (AA), namely, HFBA-*co*-AA. The PFSA/HFBA-*co*-AA blended membrane was prepared by directly mixing PFSA and HFBA-*co*-AA solution with a specific mass ratio under continuous string at room temperature. The mixture was then directly poured into a PTFE mold and dried in the oven at 150 °C for 60 min. An illustration of the preparation of PFSA/HFBA-*co*-AA membrane has been presented in Figure 1a. The molecular weight and the distribution of molecular weight are evaluated by gel permeation chromatography (GPC). Based on the results in Figure 1b, the average molecular weight (Mw) for HFBA-*co*-

https://doi.org/10.1021/acsomega.4c02263
ACS Omega 2024, 9, 26316−26324

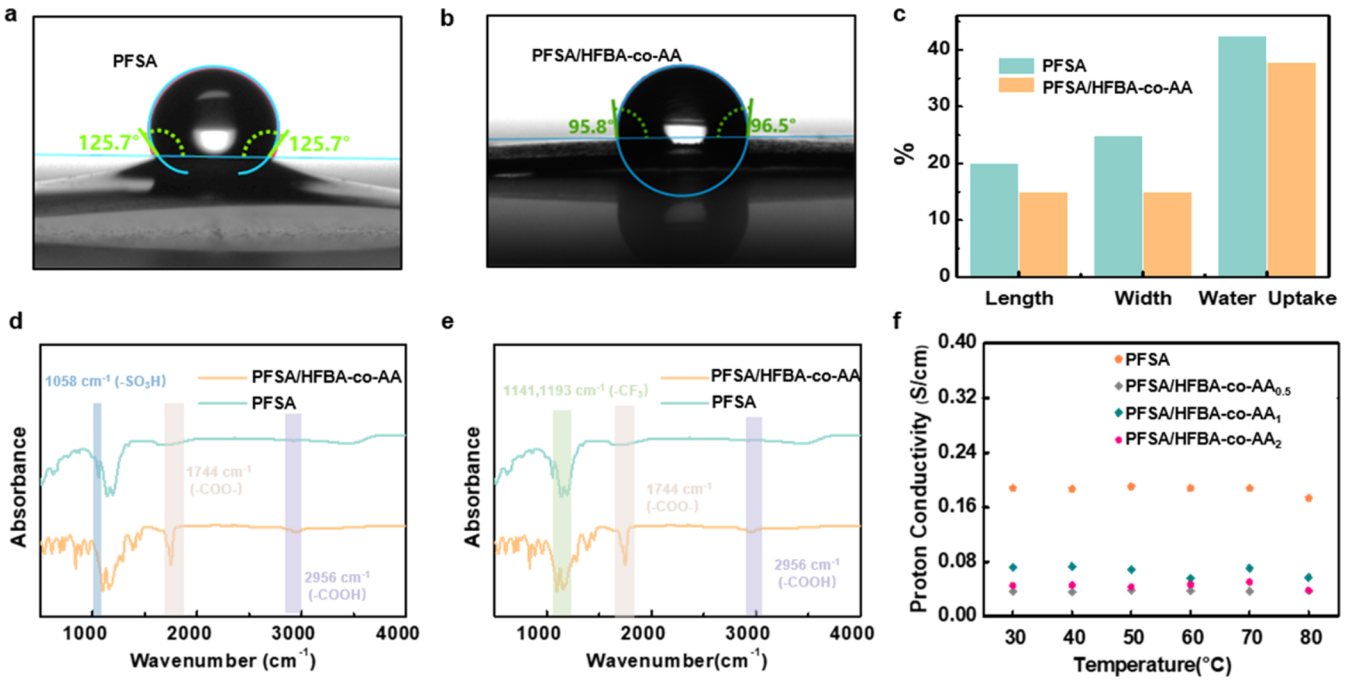

Figure 2. Shapes of water droplets (2 μL) on the (a) PFSA membrane and (b) PFSA/HFBA-*co*-AA membrane. (c) Swelling and water uptake of the PFSA membrane and PFSA/HFBA-*co*-AA membrane. (d, e) ART patterns of PFSA, PFSA/HFBA-*co*-AA membranes (same curves with different highlighted peak areas). (f) Temperature-dependent proton conductivity of the PFSA, PFSA/HFBA-*co*-$AA_{0.5}$, PFSA/HFBA-*co*-AA_1, and PFSA/HFBA-*co*-AA_2 membranes at 98%RH.

AA is 133918 g/mol, and the number-average molecular weight (Mn) is 18292 g/mol. In addition, Figure S2 shows the attenuated total refraction (ATR) spectra of PFSA and HFBA-*co*-AA. A new valley value appears at 2956 cm^{-1} in HFBA-*co*-AA, assigned to carboxyl groups (−COOH), suggesting that AA is successfully bonded with the HFBA chains. The above results support that the HFBA and AA are polymerized successfully. On the other hand, a characteristic ATR valley value at 1744 cm^{-1} can be observed, which belongs to the ester groups (−COO−) of HFBA-*co*-AA; after introducing HFBA-*co*-AA into PFSA, the blended PFSA/HFBA-*co*-AA membrane also exhibits the same valley value at 1744 cm^{-1}, suggesting the successful incorporation of HFBA-*co*-AA in PFSA (Figure S3, Supporting Information).

A series of characterizations are then conducted to explore some important features of the as-prepared PFSA/HFBA-*co*-AA membranes. Interestingly, the PFSA/HFBA-*co*-AA membrane is flexible, homogeneous, transparent, and free of megascopic defects. As shown in Figure S4a (Supporting Information), the PFSA/HFBA-*co*-AA membrane has high transparency. Specifically, the average transmittance of the ∼100 μm membrane is higher than 70% in the visible light region (400−700 nm) (Figure S4b, Supporting Information). The thickness of this membrane is higher than that of the commercialized PEM as the healing agent distribution per unit area is higher, and the mechanical strength is better. However, it should be noted that we are still pursuing an advanced membrane casting method to control thinner membranes. The elemental mapping of PFSA/HFBA-*co*-AA shows a uniform distribution of S elements, indicating that PFSA and HFBA-*co*-AA form a relatively homogeneous phase (Figure S5, Supporting Information). As shown in Figure 1c,1d, the atomic force microscope (AFM) results demonstrate that the PFSA/HFBA-*co*-AA membrane is even smoother than the pristine PFSA membranes. Accordingly, the root-mean-square roughness (R_q) measured on a surface area of 2.25 μm^2 is 22.4 and 51.8 nm for PFSA/HFBA-*co*-AA membrane and PFSA membrane, respectively (see details in Figure S6, Supporting Information).

In addition to the above features, we also focus on the hydrophilicity and the water uptake (WU) of the membrane. It is well-known that water is essential for proton conduction in PEMs since water acts as a carrier for proton movement [15]. As shown in Figure 2a,2b, the water contact angle of the PFSA/HFBA-*co*-AA membrane is lower than PFSA membrane, confirming the hydrophilic nature of HFBA-*co*-AA (see more details in Figure S7, Supporting Information). However, excessive water uptake can result in dimensional swelling and the failure of the PEMs.[6,39−42] Therefore, controlling the water uptake is important for PEMs. The water uptake capacity and dimensional stability of the PFSA and PFSA/HFBA-*co*-AA membranes are investigated. As shown in Figure 2c, the PFSA membrane presents a higher 42.58% water uptake at 80 °C while that of PFSA/HFBA-*co*-AA membrane is only 37.84% (see experimental section for details). Specifically, the length and width of the PFSA membrane increase by about 25 and 20%, respectively, after immersing in 80 °C water for 1 h; meanwhile, those of the PFSA/HFBA-*co*-AA membrane increase by 15 and 15%. In this regard, less water uptake and swelling likely demonstrate improved mechanical stability of the PFSA/HFBA-*co*-AA membranes. This could be due to the synergy between HFBA-*co*-AA complexation and the hydrophobicity of $-CF_3$ groups in HFBA (Figure 2d).

Proton conductivity is one of the crucial parameters in determining the application of PFSA/HFBA-*co*-AA membranes in PEM fuel cells.[43] In Figure 2d,2e, the ATR spectrum of PFSA membrane shows a characteristic valley value at 1058 cm^{-1}, which is ascribed to the symmetric stretching vibration

https://doi.org/10.1021/acsomega.4c02263
ACS Omega 2024, 9, 26316−26324

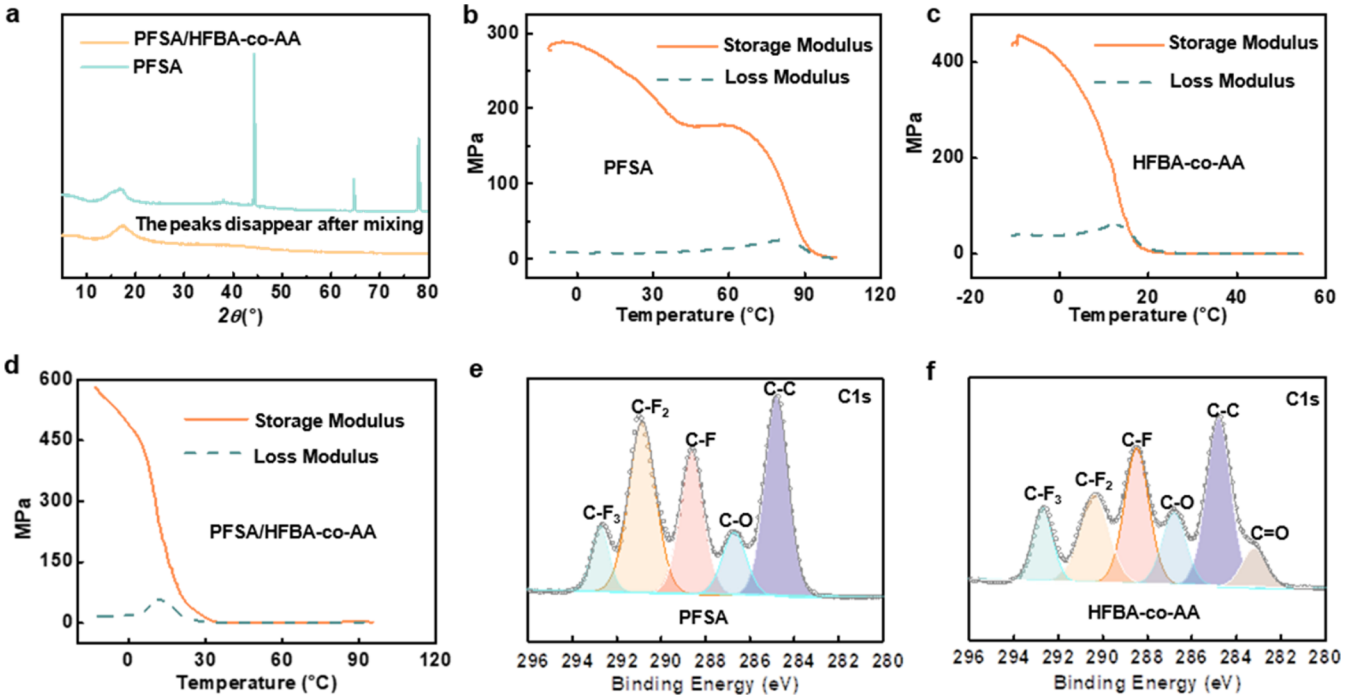

Figure 3. (a) XRD patterns of PFSA and PFSA/HFBA-*co*-AA membranes. The storage modulus (E′) and loss modulus (E″) of (b) PFSA, (c) PFSA/HFBA-*co*-AA elastomer, and (d) PFSA/HFBA-*co*-AA as a function of temperature. XPS spectra of the (e) PFSA membrane and (f) HFBA-*co*-AA membranes.

of $-SO_3H$ groups; the vibration bonds of PFSA at 1058 and 522 cm^{-1} belong to O═S═O and S−O bonds of $-SO_3H$ groups. The as-prepared PFSA/HFBA-*co*-AA membrane also shows the same valley value, indicating the same $-SO_3H$ groups inside. Normally, the $-SO_3H$ group can attract water under PEM fuel cell working conditions and aggregate to form ionic clusters where water and proton transport.[5] Therefore, both PFSA and PFSA/HFBA-*co*-AA have proton conductivity abilities. Moreover, the characteristic valley values at 1141 and 1193 cm^{-1} of PFSA/HFBA-*co*-AA are related to the symmetric stretching vibration of $-CF_3$ groups, which enables self-healing features, as discussed above.

In general, the proton conductivity of PEMs strongly depended on their water uptake and channel structures.[44] Therefore, we also study the effects of the weight ratio of PFSA to HFBA-*co*-AA on the membrane performance. This ratio is tuned as 0.5, 1, and 2, and hence, the corresponding membranes are named PFSA/HFBA-*co*-$AA_{0.5}$ ($P/H_{0.5}$), PFSA/HFBA-*co*-AA_1 (P/H_1), and PFSA/HFBA-*co*-AA_2 (P/H_2), respectively. Figure 2f presents the temperature-dependent proton conductivity of PFSA, $P/H_{0.5}$, P/H_1, and P/H_2 membranes under 98% RH. The corresponding Nyquist plots of different membranes are shown in Figure S8 (Supporting Information). It is clear that the PFSA/HFBA-*co*-AA membranes exhibit proton conductivity under different measurement conditions, although their proton conductivity is still lower than that of PFSA. These results suggest that the added self-healing filler, i.e., HFBA-*co*-AA, can decrease the proton exchangeability. As discussed in the introduction part, the PEM at the joint area between the frame and gas diffusion layer significantly suffers from degradation, where high proton conductivity is not required. In this regard, decreased proton conductivity is acceptable if we set self-healing and improved stability as the priority. Specifically, the P/H_1 membrane has higher conductivity as compared to the other two samples. This encourages us to further explore strategies to improve the proton conductivity in future studies. In the following discussion, we primarily focus on the self-healing properties of the PFSA/HFBA-*co*-AA membrane.

Usually, a polymer membrane contains both crystalline and amorphous regions. For a self-healing membrane, the amorphous regions are preferred, because the chains are relatively free inside, so that the bond formation, i.e., the self-healing process, requires lower activation energy. By contrast, few free chain segments are in the crystal regions, leading to a weak self-healing ability. To evaluate the crystallinity of our PFSA/HFBA-*co*-AA membrane, we carried out X-ray diffraction (XRD) was carried out. As shown in Figure 3a, it is clear that the peaks for PFSA disappear after mixing the self-healing HFBA-*co*-AA. This result indicates free volume in the PFSA/HFBA-*co*-AA membrane, benefiting the freedom of polymer chains inside. It is thus expected that the PFSA/HFBA-*co*-AA membrane has a better self-healing ability than the PFSA membranes.

Besides, a specific temperature is required for the self-healing process. Usually, a temperature higher than the glass transition temperature (T_g) is needed for crack healing in membrane because the free volume and polymer segmental motion are enhanced at such a high temperature. In this regard, lower T_g benefits the self-healing feature. Accordingly, dynamic thermomechanical analysis (DMA) is conducted to evaluate the storage modulus (E′) and loss modulus (E″) of PFSA/HFBA-*co*-AA membranes as a function of temperature (Figure 3b,d). The comparable E′ and E″ indicate a possible self-healing process at a specific temperature. In this work, the temperature-dependent rheology curve in Figure 3b shows that the PFSA membranes have comparable E′ and E″ only when the temperature is higher than 90 °C, much higher than the conventional fuel cell working temperature, i.e., 80 °C. Therefore, the PFSA membrane does not have self-healing

https://doi.org/10.1021/acsomega.4c02263
ACS Omega 2024, 9, 26316−26324

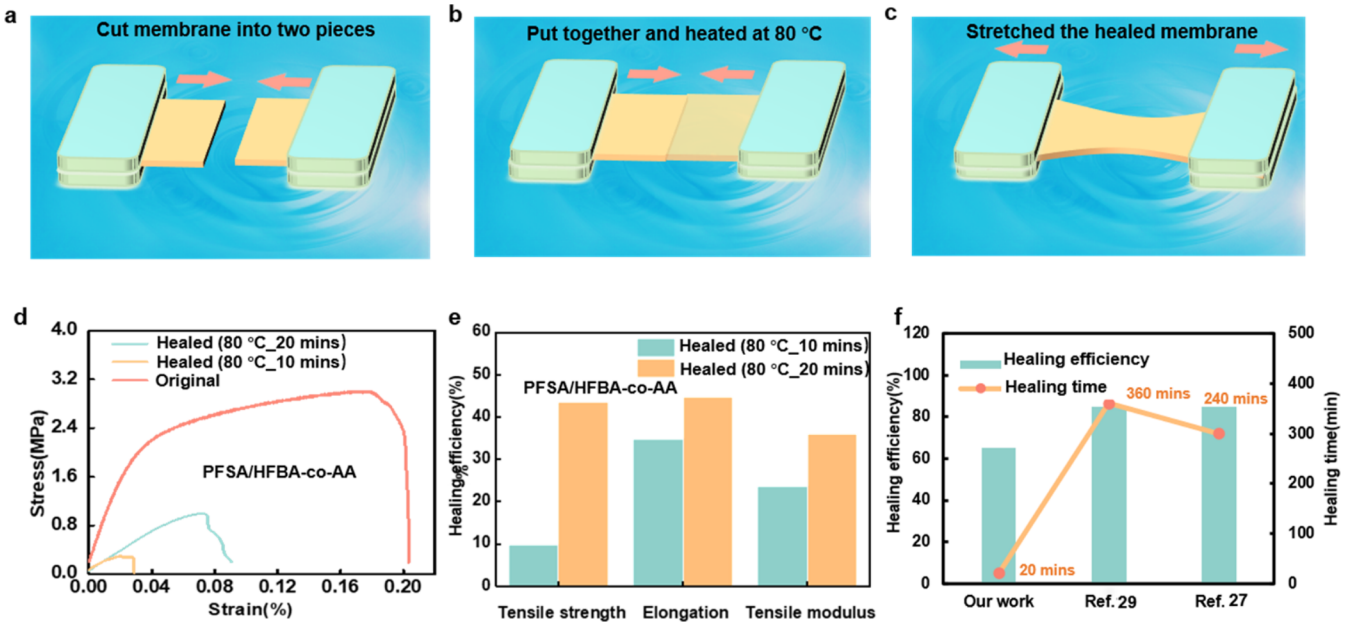

Figure 4. Schematic illustration of the self-healing process: (a) cutting the membrane into two pieces; (b) two precut membranes were put together and heated in the oven without any other treatment. (c) the healed samples were stretched (d) stress−strain curves of PFSA/HFBA-*co*-AA before and after healing at 80 °C for 10 Is. (e) bar chart of repair efficiency of PFSA/HFBA-*co*-AA before and after healing at 80 °C for 10 and 20 min. (f) Comparison of healing efficiency of PFSA/HFBA-*co*-AA with that of recently reported self-healing PEMs. The data were taken from refs 27,29.

ability under normal working conditions. Interestingly, the intersection points "E′" and "E″" curves for both HFBA-*co*-AA (Figure 3c) and PFSA/HFBA-*co*-AA (Figure 3d) membranes indicate much lower temperature than the 80 °C. These results support that the as-prepared PFSA/HFBA-*co*-AA membrane likely presents excellent self-healing ability even at room temperature.

Other than the above physical characterizations, the chemical properties of the PFSA/HFBA-*co*-AA membrane also suggest a good self-healing ability. As mentioned before, $-CF_3$ is beneficial to self-healing, as shown in Figure 3e,3f; XPS results indicate both PFSA and HFBA-*co*-AA contain $-CF_3$ group. Moreover, in Figure S9 (Supporting Information), PFSA/HFBA-*co*-AA membrane presents a negatively shifted ATR valley value (assigned to $-SO_3H$) from 1058 to 1053 cm^{-1}, compared to the PFSA membrane, demonstrating that the H-bonding interactions between $-SO_3H$ groups of PFSA and −COOH groups of AA.[45] H-bonding is one of the strongest noncovalent interactions. Owing to its reversibility, the H-bonding is highly desired in self-healing polymers.[46] Therefore, the existence of H-bonding in the PFSA/HFBA-*co*-AA membrane might synergistically improve the self-healing performance.

To visually evaluate the self-healing ability, a mechanical analysis is carried out before and after damaging the membranes.[47−51] To be specific, the PFSA/HFBA-*co*-AA membrane is first cut into two pieces, and then the fracture surfaces of these two parts are contacted at 80 °C without pressure, to allow molecular-level physical and/or chemical self-healing (Figure 4a−4c). Figure 4d shows the typical stress−strain curves of the initial PFSA/HFBA-*co*-AA membrane and those after self-healing for 10 and 20 min. The detailed data are presented in Figure 4e. Noticeably, compared to the initial uncut sample, the PFSA/HFBA-*co*-AA membrane could recover ≈9.7% in tensile strength after self-healing for 10 min; impressively, this tensile strength can be recovered for up to 43.6% if the self-healing process lasts for 10 more mins, i.e., 20 min in total.

Compared to the reported self-healing efficiency of typical PEMs, the developed PFSA/HFBA-*co*-AA membrane has demonstrated great promise (Figure 4f), suggesting that the membrane in this work is quick responding. Three possible mechanisms of the self-healing process can be identified: (1) dipole−dipole interactions ($-CF_3$ in PFSA and HFBA-*co*-AA) to enhance the cohesive-energy density (CED) at equilibrium of entangled and side-by-side copolymer chains; (2) the hydroxyl groups in AA as hydrogen donors to form dynamic reversible hydrogen bonds with the $-SO_3H$ of PFSA;[27] (3) surface-energy-driven or surface-tension-driven processes powered by interfacial energy to heal the damage.

We also performed an in situ SEM test to observe the self-healing process of the damaged PFSA/HFBA-*co*-AA membrane. As shown in Figure 5a−5c, a rip in width of several microns is made on the PFSA/HFBA-*co*-AA membrane by a razor blade prior to in situ SEM observation at 80 °C. Based on Figure 5d−5f, the scratch is gradually healed within 20 min. Particularly, at 20th min, the scratch almost disappears (Figure 5f), further confirming the quick responding and self-healing ability.

The self-healing process of the damaged PFSA/HFBA-*co*-AA is then three-dimensional (3D)-imaging in terms of depth by using a Laser Scanning Confocal Microscope. The simulated results are shown in Figure 5g−5j, while the original images and calculated depth values and self-healing efficiencies are provided in Figures S10 and S11 (Supporting Information) and Table S1 (Supporting Information). Heating at 80 °C for 10 min leads to a healing efficiency of 31.17%; if we prolong the heating time to 40 min, the healing efficiency can be above 65%.

https://doi.org/10.1021/acsomega.4c02263
ACS Omega 2024, 9, 26316−26324

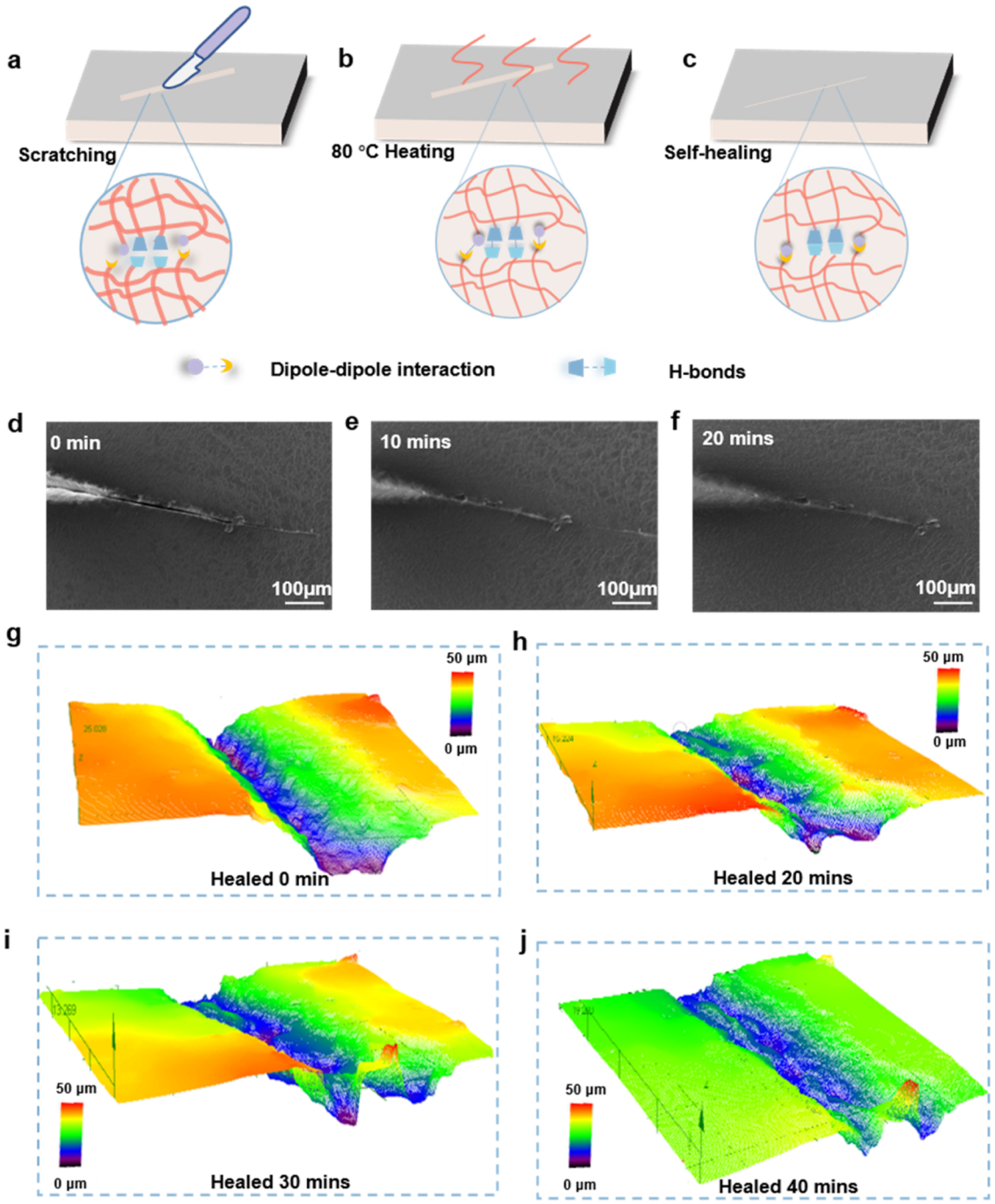

Figure 5. Schematic diagram showed the self-healing of membrane samples: (a) the crack is man-made by a sharp knife, (b) heating the membrane sample at 80 °C, and (c) after heating, the crack became narrow and even disappeared. The SEM images illustrate a cracked PFSA/HFBA-*co*-AA membrane sample before and after self-healing, and a reference is placed for observation. After heating the membrane sample at 80 °C for (d) 0 min, and (e) 10 min, the crack partly disappeared. As the control, PFSA/HFBA-*co*-AA membrane was treated with the same procedure while the surface was healing at 80 °C for (f) 20 min. Schematics showing the self-healing of membrane samples by a laser scanning confocal microscope. Laser Scanning Confocal Microscope images of the PFSA/HFBA-*co*-AA membrane during the self-healing process: (g) original, (h) healing for 20 min, (i) healing for 30 min, (j) healing for 40 min.

3. CONCLUSIONS

In summary, we have developed ultrastable, quick responding, and self-healing PEMs by dipole interactions and hydrogen bonding complexation between PFSA and HFBA-*co*-AA. Resulting from the dynamically reversible hydrogen bonding network and dynamically reversible dipole−dipole in the polymer network, the blended PFSA/HFBA-*co*-AA membrane exhibited mechanical strength stability and excellent healing ability. Furthermore, hydrophilic nanochannels by AA are provided, which can offer the water nanochannels for proton conductivity of the blended membrane (0.07 S/cm at 40 °C-98% RH and 0.071 S/cm at 70 °C-98% RH). Particularly, it shows excellent self-healing properties; for example, 43.6% of the original tensile strength can be recovered within only 20 min at 80 °C. As a versatile solid-state electrolyte for fuel cells, this PEM presented excellent healing properties and durability.

https://doi.org/10.1021/acsomega.4c02263
ACS Omega 2024, 9, 26316−26324

This intrinsic self-healing integration strategy intercalation proposed here allows the assembly of new multifunctional and high-performance PEMs under precise interfacial control, with great potential for next-generation fuel cells with high durability and long life span.

4. METHODS

Materials. Perfluorinated sulfonic acid solid particle (3M), 2,2,3,4,4,4-Hexafluorobutyl acrylate (HFBA, Aladdin, >95%), Acrylic acid (Meryer >99%). *N*,*N*-Dimethylformamide (DMF, Aladdin, >99%), *n*-propanol (NPA, Aladdin, >99%). Azodiisobutyronitrile (AIBN, Aladdin, >98%)

Synthesis HFBA-*co*-AA Polymer. 40 mmol of HFBA, 10 mmol of AA, and 0.25 mmol of AIBN were mixed in a glass bottle, stirred for 30 min, and then heated at 70 °C for 30 min. Add 10.72 g of DMF into this bottle and stir for 24 h. Specifically, 40 mmol HFBA, 10 mmol AA, and 0.25 mmol azodiisobutyronitrile (AIBN) were mixed in a glass bottle and stirred for 30 min, followed by heating at 70 °C for 30 min. Next, we added 10.72 g of *N*,*N*-Dimethylformamide (DMF) into this bottle and stirred for 24 h to prepare the HFBA-*co*-AA solution.

Fabrication of Recast PFSA Membranes. PFSA solution with a feed mass ratio of PFSA in NPA solution under continuous string at room temperature. They could form a uniform dispersion. The solution was then directly poured into a PTFE mold and dried in the oven at 150 °C for 60 min.

Fabrication of PFSA/HFBA-*co*-AA Membranes. PFSA/HFBA-*co*-AA complexes were prepared by directly mixing PFSA and HFBA-*co*-AA solution with a feed mass ratio of PFSA to HFBA-*co*-AA under a continuous string at room temperature. They could form a uniform dispersion. The mixture was then directly poured into PTFE mold, drying in the oven at 150 °C for 60 min.

Characterization and Measurements. The attenuated total refraction (ATR) was obtained on a PerkinElmer Frontier ATR spectrometer to analyze the chemical structures of PFSA, PFSA, HFBA-*co*-AA, and PFSA/HFBA-*co*-AA membranes. Scanning electron microscopy (SEM) was performed to reveal the physical morphology of the membranes. SEM was operated by Axia ChemiSEM to observe the surface and cross-section morphologies of blended PFSA/HFBA-*co*-AA membranes. Water contact angle measurements were performed at ambient temperature with a DSA-25 drop-shape analysis. The water contact angles on the membrane were measured at three different points on each membrane within 1s of contact with water droplets. An electromechanical universal testing machine (EUTM) (Instron 5943) was used to obtain the mechanical properties of the as-prepared membrane (overall length: 40 mm; width: 6 mm) at 5 mm/min tensile speed at room temperature (25 °C). Three replicates of each sample were tested to reduce the error.

The water uptake (WU) and volume dimensional swelling (VS) of membranes were determined by measuring changes in their weight and volume between the dried and wet states. Membranes were first dried with the wet membranes at 60 °C in a vacuum oven for 12 h, and the weight and the volume of dried membranes were measured immediately. Then, the mixture was immersed in deionized water at 80 °C for 1 h. Then, the weight and volume of wet membranes were quickly recorded after gently wiping water from the surface. The WU and VS of membranes were calculated as follows

$$\mathrm{WU} = \frac{(W_{\mathrm{wet,w}} - W_{\mathrm{dry}})}{W_{\mathrm{dry}}} \times 100\%$$

where $W_{\mathrm{wet,w}}$, and W_{dry} are weights of wet (in water) and dried membranes, respectively.

$$\mathrm{VS} = \frac{W_{\mathrm{wet,w}} - V_{\mathrm{dry}}}{V_{\mathrm{dry}}} \times 100\%$$

where $V_{\mathrm{wet,w}}$, and V_{dry} are the volumes of wet and dry membranes, respectively.

The proton conductivity was measured on a RST 5000 potentiostat/frequency-response analyzer (FRA) by a two-electrode AC impedance method from 1 Hz to 1 MHz. Test samples were 2.5 cm wide and 2.5 cm long. All samples were kept at 98% RH for 1 h to equilibrate to the test conditions prior to testing. The proton conductivity was calculated by the following equation

$$\sigma = \frac{d}{Rtw}$$

where σ is the proton conductivity (S/cm) of the membranes, d is the distance between the electrodes (cm), and t and w are the thickness (cm) and width (cm) of the membranes, respectively. R is the resistance from the impedance data (Ω).

■ ASSOCIATED CONTENT

Data Availability Statement

Data are available throughout the manuscript and supporting files.

Supporting Information

The Supporting Information is available free of charge at https://pubs.acs.org/doi/10.1021/acsomega.4c02263.

Comparison between this work and publications; digital pictures; physical characterizations of PEMs in terms of surface chemistry and morphology; features during self-healing processes (PDF)

■ AUTHOR INFORMATION

Corresponding Authors

Lixin Xing − *Huangpu Hydrogen Energy Innovation Centre/School of Chemistry and Chemical Engineering, Guangzhou University, Guangzhou 510006, P. R. China;* Email: lixinxing@gzhu.edu.cn

Siyu Ye − *Huangpu Hydrogen Energy Innovation Centre/School of Chemistry and Chemical Engineering, Guangzhou University, Guangzhou 510006, P. R. China; SinoHykey Technology Guangzhou Co., Ltd., Guangzhou 510530, P. R. China;* orcid.org/0000-0002-4384-5025; Email: siyu.ye@gzhu.edu.cn

Authors

Shanyun Mo − *Huangpu Hydrogen Energy Innovation Centre/School of Chemistry and Chemical Engineering, Guangzhou University, Guangzhou 510006, P. R. China; SinoHykey Technology Guangzhou Co., Ltd., Guangzhou 510530, P. R. China*

Zihui Li − *Huangpu Hydrogen Energy Innovation Centre/School of Chemistry and Chemical Engineering, Guangzhou University, Guangzhou 510006, P. R. China*

https://doi.org/10.1021/acsomega.4c02263
ACS Omega 2024, 9, 26316−26324

Junda Chen − *Huangpu Hydrogen Energy Innovation Centre/School of Chemistry and Chemical Engineering, Guangzhou University, Guangzhou 510006, P. R. China*
Yue Chen − *Huangpu Hydrogen Energy Innovation Centre/School of Chemistry and Chemical Engineering, Guangzhou University, Guangzhou 510006, P. R. China*
Ning Wang − *Huangpu Hydrogen Energy Innovation Centre/School of Chemistry and Chemical Engineering, Guangzhou University, Guangzhou 510006, P. R. China*
Chunmei Tang − *Huangpu Hydrogen Energy Innovation Centre/School of Chemistry and Chemical Engineering, Guangzhou University, Guangzhou 510006, P. R. China*
Ling Meng − *Huangpu Hydrogen Energy Innovation Centre/School of Chemistry and Chemical Engineering, Guangzhou University, Guangzhou 510006, P. R. China*
Lei Du − *Huangpu Hydrogen Energy Innovation Centre/School of Chemistry and Chemical Engineering, Guangzhou University, Guangzhou 510006, P. R. China*

Complete contact information is available at: https://pubs.acs.org/10.1021/acsomega.4c02263

Author Contributions

S.M. contributed to conceptualization, methodology, investigation, and writing original draft. Z.L. contributed to investigation and software. J.C. contributed to investigation and software. Y.C. contributed to investigation and software. N.W. contributed to writing review and editing. C.T. contributed to writing review and editing. L.M. contributed to writing review and editing. L.D. contributed to writing review and editing and funding acquisition. L.X. contributed to conceptualization and writing review and editing. S.Y. contributed to conceptualization, writing review and editing, and funding acquisition.

Notes

The authors declare no competing financial interest.

■ ACKNOWLEDGMENTS

This work was supported by the National Natural Science Foundation of China (22250710133 and 51803042), Outstanding Youth Project of Natural Science Foundation of Guangdong Province (2022B1515020020), Guangzhou University Graduate Student Innovation Ability Cultivation Funding Scheme (2022GDJC-M11), the Science and Technology Projects in Guangzhou (2024A03J0308), Basic and Applied Basic Research Foundation of Guangdong Province (2022B1515120079) and Guangdong Engineering Technology Research Center for Hydrogen Energy and Fuel Cells.

■ REFERENCES

(1) Ishimoto, T.; Koyama, M. A review of molecular-level mechanism of membrane degradation in the polymer electrolyte fuel cell. *Membranes* **2012**, *2*, 395−414.
(2) Fan, J.; Chen, M.; Zhao, Z.; Zhang, Z.; Ye, S.; Xu, S.; Wang, H.; Li, H. Bridging the gap between highly active oxygen reduction reaction catalysts and effective catalyst layers for proton exchange membrane fuel cells. *Nat. Energy* **2021**, *6*, 475−486.
(3) Banham, D.; Zou, J.; Mukerjee, S.; Liu, Z.; Yang, D.; Zhang, Y.; Peng, Y.; Dong, A. Ultralow platinum loading proton exchange membrane fuel cells: Performance losses and solutions. *J. Power Sources* **2021**, *490*, No. 229515.
(4) Suter, T. A. M.; Smith, K.; Hack, J.; Rasha, L.; Rana, Z.; Angel, G. M. A.; Shearing, P. R.; Miller, T. S.; Brett, D. J. L. Engineering Catalyst Layers for Next-Generation Polymer Electrolyte Fuel Cells: A Review of Design, Materials, and Methods. *Adv. Energy Mater.* **2021**, *11*, No. 2101025.
(5) Karimi, M. B.; Mohammadi, F.; Hooshyari, K. Recent approaches to improve Nafion performance for fuel cell applications: A review. *Int. J. Hydrogen Energy* **2019**, *44*, 28919−28938.
(6) Wang, Y.; Chen, K. S.; Mishler, J.; Cho, S. C.; Adroher, X. C. A review of polymer electrolyte membrane fuel cells: Technology, applications, and needs on fundamental research. *Appl. Energy* **2011**, *88*, 981−1007.
(7) Bose, S.; Kuila, T.; Nguyen, T. X. H.; Kim, N. H.; Lau, K.-t.; Lee, J. H. Polymer membranes for high temperature proton exchange membrane fuel cell: Recent advances and challenges. *Prog. Polym. Sci.* **2011**, *36*, 813−843.
(8) Rosli, R. E.; Sulong, A. B.; Daud, W. R. W.; Zulkifley, M. A.; Husaini, T.; Rosli, M. I.; Majlan, E. H.; Haque, M. A. A review of high-temperature proton exchange membrane fuel cell (HT-PEMFC) system. *Int. J. Hydrogen Energy* **2017**, *42*, 9293−9314.
(9) Kusoglu, A.; Weber, A. Z. New Insights into Perfluorinated Sulfonic-Acid Ionomers. *Chem. Rev.* **2017**, *117*, 987−1104.
(10) Nguyen, H.; Klose, C.; Metzler, L.; Vierrath, S.; Breitwieser, M. Fully Hydrocarbon Membrane Electrode Assemblies for Proton Exchange Membrane Fuel Cells and Electrolyzers: An Engineering Perspective. *Adv. Energy Mater.* **2022**, *12*, No. 2103559.
(11) Sriruangrungkamol, A.; Chonkaew, W. Modification of nanocellulose membrane by impregnation method with sulfosuccinic acid for direct methanol fuel cell applications. *Polym. Bull.* **2021**, *78*, 3705−3728.
(12) Liu, X.; Li, Y.; Xue, J.; Zhu, W.; Zhang, J.; Yin, Y.; Qin, Y.; Jiao, K.; Du, Q.; Cheng, B.; Zhuang, X.; Li, J.; Guiver, M. D. Magnetic field alignment of stable proton-conducting channels in an electrolyte membrane. *Nat. Commun.* **2019**, *10*, No. 842.
(13) Devrim, Y.; Devrim, H. PEM fuel cell short stack performances of silica doped nanocomposite membranes. *Int. J. Hydrogen Energy* **2015**, *40*, 7870−7878.
(14) Quartarone, E.; Angioni, S.; Mustarelli, P. Polymer and Composite Membranes for Proton-Conducting, High-Temperature Fuel Cells: A Critical Review. *Materials* **2017**, *10*, 687.
(15) Yoon, K. R.; Lee, K. A.; Jo, S.; Yook, S. H.; Lee, K. Y.; Kim, I. D.; Kim, J. Y. Mussel-Inspired Polydopamine-Treated Reinforced Composite Membranes with Self-Supported CeO_x Radical Scavengers for Highly Stable PEM Fuel Cells. *Adv. Funct. Mater.* **2018**, *29*, No. 1806929, DOI: 10.1002/adfm.201806929.
(16) Kienitz, B.; K, J.; Priester, S.; Baczkowski, C. Ultra-Thin Reinforced Ionomer mbranes to Meet Next Generation Fuel Cell Targets. *ECS Trans.* **2011**, *41*, 1521−1530, DOI: 10.1149/1.3635683.
(17) Liu, Y. R.; Chen, Y. Y.; Zhuang, Q.; Li, G. Recent advances in MOFs-based proton exchange membranes. *Coord. Chem. Rev.* **2022**, *471*, No. 214740.
(18) Pandey, R. P.; Shukla, G.; Manohar, M.; Shahi, V. K. Graphene oxide based nanohybrid proton exchange membranes for fuel cell applications: An overview. *Adv. Colloid Interface Sci.* **2017**, *240*, 15−30.
(19) Zhang, T.; Wang, P.; Chen, H.; Pei, P. A review of automotive proton exchange membrane fuel cell degradation under start-stop operating condition. *Appl. Energy* **2018**, *223*, 249−262.
(20) Wang, Y.; Diaz, D. F. R.; Chen, K. S.; Wang, Z.; Adroher, X. C. Materials, technological status, and fundamentals of PEM fuel cells − A review. *Mater. Today* **2020**, *32*, 178−203, DOI: 10.1016/j.mattod.2019.06.005.
(21) Liu, W.; Qiu, D.; Peng, L.; Yi, P.; Lai, X. Mechanical degradation of proton exchange membrane during assembly and running processes in proton exchange membrane fuel cells with metallic bipolar plates. *Int. J. Hydrogen Energy* **2020**, *44*, 8622−8634.
(22) Qiu, D.; Peng, L.; Liang, P.; Yi, P.; Lai, X. Mechanical degradation of proton exchange membrane along the MEA frame in proton exchange membrane fuel cells. *Energy* **2018**, *165*, 210−222.
(23) Ren, P.; Pei, P.; Li, Y.; Wu, Z.; Chen, D.; Huang, S. Degradation mechanisms of proton exchange membrane fuel cell

under typical automotive operating conditions. *Prog. Energy Combust. Sci.* **2020**, *80*, No. 100859.
(24) Han, M.; Shul, Y.-G.; Lee, H.; Shin, D.; Bae, B. Accelerated testing of polymer electrolyte membranes under open-circuit voltage conditions for durable proton exchange membrane fuel cells. *Int. J. Hydrogen Energy* **2017**, *42*, 30787−30791.
(25) Zhao, L.; Zhu, J.; Zheng, Y.; Xiao, M.; Gao, R.; Zhang, Z.; Wen, G.; Dou, H.; Deng, Y. P.; Yu, A.; Wang, Z.; Chen, Z. Materials Engineering toward Durable Electrocatalysts for Proton Exchange Membrane Fuel Cells. *Adv. Energy Mater.* **2021**, *12*, No. 2102665, DOI: 10.1002/aenm.202102665.
(26) Wang, L.; Advani, S. G.; Prasad, A. K. Self-Healing Composite Membrane for Proton Electrolyte Membrane Fuel Cell Applications. *J. Electrochem. Soc.* **2016**, *163*, F1267−F1271.
(27) Li, Y.; Liang, L.; Liu, C.; Li, Y.; Xing, W.; Sun, J. Self-Healing Proton-Exchange Membranes Composed of Nafion-Poly(vinyl alcohol) Complexes for Durable Direct Methanol Fuel Cells. *Adv. Mater.* **2018**, *30*, No. e1707146.
(28) Li, Y.; Li, Z.; Wang, W.; Sun, J. Self-healing and highly elastic fluorine-free proton exchange membranes comprised of poly(vinyl alcohol) derivative and phytic acid for durable fuel cells. *Sci. China Mater.* **2020**, *63*, 1235−1246.
(29) Zhu, L.; Li, Y.; Ye, P.; Zhao, J.; Liu, J.; Lei, J.; Wang, L.; Xue, R. Ultra-Stable, Highly Proton Conductive, and Self-Healing Proton Exchange Membranes Based On Molecule Intercalation Technique and Noncovalent Assembly Nanostructure. *Adv. Funct. Mater.* **2022**, *33*, No. 2210453, DOI: 10.1002/adfm.202210453.
(30) Ng, W. W.; Thiam, H. S.; Pang, Y. L.; Lim, Y. S.; Wong, J.Facile synthesis of nafion based self-healable proton exchange membranes for direct methanol fuel cells *Mater. Today Proc.* 2023 DOI: 10.1016/j.matpr.2023.01.407.
(31) Zhu, Y.; Yin, T.; Ren, J.; Liu, C.; Fu, D.; Ge, L. Self-healing polyelectrolyte multilayer composite film with microcapsules. *RSC Adv.* **2016**, *6*, 12100−12106.
(32) Zhu, Y.; Xuan, H.; Ren, J.; Liu, X.; Zhao, B.; Zhang, J.; Ge, L. Humidity responsive self-healing based on intermolecular hydrogen bonding and metal−ligand coordination. *RSC Adv.* **2016**, *6*, 89757−89763.
(33) Bai, S.; Sun, C.; Yan, H.; Sun, X.; Zhang, H.; Luo, L.; Lei, X.; Wan, P.; Chen, X. Healable, Transparent, Room-Temperature Electronic Sensors Based on Carbon Nanotube Network-Coated Polyelectrolyte Multilayers. *Small* **2015**, *11*, 5807−5813.
(34) Gaynor, J.; Gregory, S.; Paul, S.; Julie, P. H. Effects of Fluorinated Substituents on the Refractive Index and Optical Radiation Resistance of Methacrylates. *J. Appl. Polym.* **1993**, *50*, 1645−1653.
(35) O'Hagan, D. Understanding organofluorine chemistry. An introduction to the C-F bond. *Chem. Soc. Rev.* **2008**, *37*, 308−319.
(36) Liu, Y.; Chen, T.; Jin, Z.; Li, M.; Zhang, D.; Duan, L.; Zhao, Z.; Wang, C. Tough, stable and self-healing luminescent perovskite-polymer matrix applicable to all harsh aquatic environments. *Nat. Commun.* **2022**, *13*, No. 1338.
(37) Kalista, S. J.; Pflug, J. R.; Varley, R. J. Effect of ionic content on ballistic self-healing in EMAA copolymers and ionomers. *Polym. Chem.* **2013**, *4*, 4910−4926.
(38) Wang, Z.; Tao, F.; Pan, Q. A self-healable polyvinyl alcohol-based hydrogel electrolyte for smart electrochemical capacitors. *J. Mater. Chem. A* **2016**, *4*, 17732−17739.
(39) Qiu, D.; Peng, L.; Lai, X.; Ni, M.; Lehnert, W. Mechanical failure and mitigation strategies for the membrane in a proton exchange membrane fuel cell. *Renewable Sustainable Energy Rev.* **2019**, *113*, No. 109289.
(40) Pourzare, K.; Mansourpanah, Y.; Farhadi, S. Advanced nanocomposite membranes for fuel cell applications: a comprehensive review. *Biofuel Res. J.* **2016**, *3*, 496−513.
(41) Jiang, Z.; Jiang, Z.-J. Plasma techniques for the fabrication of polymer electrolyte membranes for fuel cells. *J. Membr. Sci.* **2014**, *456*, 85−106.
(42) Wong, C. Y.; Wong, W. Y.; Ramya, K.; Khalid, M.; Loh, K. S.; Daud, W. R. W.; Lim, K. L.; Walvekar, R.; Kadhum, A. A. H. Additives in proton exchange membranes for low- and high-temperature fuel cell applications: A review. *Int. J. Hydrogen Energy* **2019**, *44*, 6116−6135.
(43) Shin, D. W.; Guiver, M. D.; Lee, Y. M. Hydrocarbon-Based Polymer Electrolyte Membranes: Importance of Morphology on Ion Transport and Membrane Stability. *Chem. Rev.* **2017**, *117*, 4759−4805.
(44) Qu, E.; Hao, X.; Xiao, M.; Han, D.; Huang, S.; Huang, Z.; Wang, S.; Meng, Y. Proton exchange membranes for high temperature proton exchange membrane fuel cells: Challenges and perspectives. *J. Power Sources* **2022**, *533*, No. 231386.
(45) Liu, J.; Long, J.; Shen, Z.; Jin, X.; Han, T.; Si, T.; Zhang, H. A Self-Healing Flexible Quasi-Solid Zinc-Ion Battery Using All-In-One Electrodes. *Adv. Sci.* **2021**, *8*, No. 2004689.
(46) Yao, Y.; Xu, Z.; Liu, B.; Xiao, M.; Yang, J.; Liu, W. Multiple H-Bonding Chain Extender-Based Ultrastiff Thermoplastic Polyurethanes with Autonomous Self-Healability, Solvent-Free Adhesiveness, and AIE Fluorescence. *Adv. Funct. Mater.* **2020**, *31*, No. 2006944, DOI: 10.1002/adfm.202006944.
(47) Huang, Z. K.; Deng, Z. S.; Liu, X.; Huang, T. R.; Hu, Y. J.; Chen, Y. T.; Liu, Y. H.; Guo, Z. H.; Yue, K. Highly stretchable, strain-stiffening, self-healing ionic conductors for wearable sensors. *Chem. Eng. J.* **2022**, *449*, No. 137633.
(48) Qu, X. X.; Niu, W. W.; Wang, R.; Li, Z. Q.; Guo, Y.; Liu, X. K.; Sun, J. Q. Solid-state and liquid-free elastomeric ionic conductors with autonomous self-healing ability. *Mater. Horiz.* **2020**, *7*, 2994−3004.
(49) Huang, H.; Han, L.; Fu, X.; Wang, Y.; Yang, Z.; Pan, L.; Xu, M. A Powder Self-Healable Hydrogel Electrolyte for Flexible Hybrid Supercapacitors with High Energy Density and Sustainability. *Small* **2021**, *17*, No. e2006807.
(50) Wang, S.; Urban, M. W. Self-healing polymers. *Nat. Rev. Mater.* **2020**, *5*, 562−583.
(51) Li, B.; Cao, P. F.; Saito, T.; Sokolov, A. P. Intrinsically Self-Healing Polymers: From Mechanistic Insight to Current Challenges. *Chem. Rev.* **2023**, *123*, 701−735.

https://doi.org/10.1021/acsomega.4c02263
ACS Omega 2024, 9, 26316−26324